IJIE

UTHM Penerbit

INTERNATIONAL JOURNAL OF INTEGRATED ENGINEERING
ISSN: 2229-838X e-ISSN: 2600-7916

Vol. 18 No. 3 (2026) 31-47
https://publisher.uthm.edu.my/ojs/index.php/ijie

CFD Analysis of Motorcycle Moving on Bridge During Overtaking Under Crosswind Conditions

Tiong Woei Ting[1], Izuan Amin Ishak[1]*, Mohammad Arafat[1], Nofrizalidris Darlis[1], Nur Haziqah Shaharuddin[2], Ahmad Faiz Mohammad[3]

[1] *Department of Mechanical Engineering Technology, Faculty of Engineering Technology, Universiti Tun Hussein Onn Malaysia (UTHM), 84600 Pagoh, Johor, MALAYSIA*

[2] *Department of Mechanical Engineering, Keio University, Yokohama, JAPAN*

[3] *Department of Mechanical Precision Engineering, Malaysia-Japan International Institute of Technology (MJIIT), Universiti Teknologi Malaysia (UTM), Jalan Sultan Yahya Petra, 54100, Kuala Lumpur, MALAYSIA*

*Corresponding Author: izuan@uthm.edu.my
DOI: https://doi.org/10.30880/ijie.2026.18.03.003

Article Info

Received: 19 September 2025
Accepted: 30 December 2025
Available online: 30 April 2026

Keywords

Aerodynamic coefficients, ANSYS Fluent, crosswind, Computational Fluid Dynamics (CFD), flow structures, overtaking maneuvers

Abstract

This study examines the aerodynamic challenges faced by motorcycles during overtaking maneuvers on bridges under crosswind conditions, addressing a critical safety issue often overlooked in existing research, which primarily focuses on cars. With over 20,000 motorcyclists traversing the Penang Bridge daily and exposed to crosswinds reaching 18.5 km/h, the risks of accidents due to aerodynamic instability are significant. Using Computational Fluid Dynamics (CFD) simulations through ANSYS Fluent, this research analyzes the aerodynamic interactions between motorcycles and overtaking vehicles under crosswind angles of 20°, 30°, 40°, and 50°. Special attention was given to resolving key flow features and accurately capturing transient aerodynamic phenomena that govern motorcycle stability, rather than relying solely on mesh refinement for solution reliability. Aerodynamic coefficients, including drag, lift, and side force, were evaluated during various phases of the overtaking process. The results reveal that crosswinds at a yaw angle of 50° increase the drag coefficient by 45% and the side force coefficient by 72% compared to baseline conditions without crosswind. These amplified aerodynamic loads substantially heighten the risk to rider stability. Conversely, the presence of an overtaking vehicle reduces drag force on the motorcycle by up to 20% due to partial shielding but introduces wake turbulence that affects lateral stability. Pressure distribution analysis shows a high-pressure concentration on the windward side, contributing significantly to lateral forces that destabilize the motorcycle. These findings offer critical insights into the behavior of motorcycles under challenging environmental conditions, emphasizing the need for enhanced bridge safety guidelines, optimized motorcycle designs, and improved rider safety strategies. This research provides a foundation for future studies on mitigating aerodynamic instability and reducing accident risks, contributing to safer motorcycle operations in crosswind-prone environments.

1. Introduction

Bridge safety during adverse environmental conditions has become a significant area of research, especially with the growing reliance on long-span bridges for transportation. Motorcycles, due to their lightweight structure, smaller frontal area, and higher susceptibility to external forces, are particularly vulnerable to aerodynamic instability. Bridges exposed to crosswinds pose unique challenges, particularly for motorcycles, which are highly susceptible to aerodynamic instability. Crosswinds, combined with aerodynamic interference during overtaking maneuvers, can create dangerous conditions for riders [1]. This study addresses the pressing need to understand the dynamics of motorcycle stability under such conditions, contributing to improved safety and design guidelines.

Crosswind conditions pose significant challenges to vehicle stability, particularly for motorcycles and other high-sided vehicles operating on exposed infrastructure like bridges. The transient nature of aerodynamic forces in crosswinds can lead to lateral instability, affecting safety and control. Numerous studies have highlighted the importance of computational fluid dynamics (CFD) in modeling these complex interactions to improve vehicle designs and predict dynamic behavior [2],[3]. These simulations provide insights into the effects of yaw angles, turbulence, and aerodynamic forces on stability [4]. Early studies explored the impact of crosswinds on vehicle aerodynamics. Lin Ma et al. [5] conducted experimental research on how crosswinds create pressure cavities behind moving vehicles, altering flow patterns and stability. Charuvisit et al. [6] used wind tunnel tests to examine how bridge towers influence transient aerodynamic forces, particularly under crosswind angles, identifying 30° as the most critical direction for instability. Fintelman et al. [7] employed numerical methods to simulate the aerodynamic effects of crosswinds on motorcycles, highlighting significant increases in rolling moments and lift forces with yaw angles. Arafat et al. [8] highlighted the crosswind angle significantly influenced aerodynamic flow behavior as the train exited the tunnel, altering surface airflow patterns and pressure distribution on the leeward and windward sides. Studies investigating crosswind effects have identified significant lateral and yaw instabilities due to sudden gusts and complex flow fields. These findings have been corroborated by experimental and CFD simulations exploring various yaw angles and vehicle types, including buses, trucks, and rail vehicles [9],[10].

Vehicle interactions during overtaking maneuvers further compound these complexities. The relative motion of vehicles introduces transient aerodynamic forces that may destabilize both vehicles involved. Overtaking scenarios under crosswind conditions have been shown to amplify lateral forces, moments, and vortices, particularly for high-sided vehicles and large passenger cars [11],[12]. Noger et al. [13] investigated the transient aerodynamic forces during overtaking, using scaled models to study how interactions between heavy and light vehicles influence stability. Corin et al. [14] analyzed quasi-steady and unsteady flow during overtaking in crosswinds, revealing discrepancies in aerodynamic force calculations between these methods. Uddin et al. [15] demonstrated through CFD simulations that overtaking vehicles experience varying aerodynamic coefficients depending on their relative velocities. Alonso et al. [16] explored how infrastructure designs like embankments and flat ground influence aerodynamic stability, with findings emphasizing that complex infrastructures exacerbate instability under crosswind conditions. Khairullah et al. [17] analyze the impact of embankment heights and crosswind angles on high-speed train aerodynamics using CFD. Higher crosswind angles worsened performance and increased leeward vortex formation.

While these studies provide valuable insights into the impact of crosswinds and vehicle interactions, the vast majority center on cars, trucks, and trains. Very few have addressed motorcycles specifically, despite their increased vulnerability due to low inertia and greater sensitivity to crosswind-induced yaw and roll moments. Despite these advances, the interaction between motorcycles and crosswinds during overtaking maneuvers remains poorly understood. Previous studies have primarily focused on cars and trucks, leaving motorcycle-specific scenarios underexplored. This lack of focused study creates a crucial gap in the literature regarding motorcycle safety on long-span bridges like the Penang Bridge, which is known to experience strong crosswinds and high motorcycle traffic. This study hypothesizes that higher crosswind angles increase aerodynamic forces, posing greater risks to stability, particularly during mid-overtaking phases.

Using Computational Fluid Dynamics (CFD) simulations, this research evaluates aerodynamic parameters across various scenarios. Parameters such as drag, lift, and side force coefficients will be analyzed for motorcycles under different crosswind conditions, including yaw angles of 20°, 30°, 40°, and 50°. The findings aim to provide critical insights into rider safety and contribute to the development of improved guidelines for bridge design and motorcycle performance in crosswind-prone environments.

2. Methodology

2.1 Model Description

The study utilizes simplified models for the motorcycle with rider [5], and SUV car [18], as well as a bridge structure [19], to investigate aerodynamic interactions. While preserving crucial geometric and aerodynamic features, simplifying the model aids in concentrating on the most important elements of the vehicle's performance. The simulations can be run more effectively because to this complexity reduction, which also saves time and computer resources [20]. The simplified geometries of the car and motorcycle were designed to capture the essential aerodynamic features while maintaining computational efficiency. While the car model does not replicate the Ahmed body, its bluff rear and slanted front surface provide comparable wake dynamics. Similarly, the motorcycle geometry was inspired by simplified forms used in prior studies [21]-[23], which aim to represent general rider-bike interactions. These geometries are not intended for direct comparison with standardized benchmarks but are suitable for assessing relative aerodynamic behavior during overtaking. The decision to use simplified models is justified by the need to balance accuracy with computational feasibility. Full-detail models of motorcycles and riders, including intricate geometry such as suspension components or helmet contours, would significantly increase mesh complexity and simulation cost, without proportionally improving the ability to analyze transient aerodynamic trends. Simplified models also reduce uncertainties related to surface detail that may vary widely among actual motorcycles, thereby supporting a more generalized understanding of aerodynamic behavior.

The rider posture used in this study represents a tucked-in racing position, which, while not typical for everyday commuting, was selected to examine a low-drag scenario often considered in aerodynamic assessments. We acknowledge that a more upright position would be more representative of real-world overtaking maneuvers. This represents one of the limitations of the simplified model, specifically, its reduced ability to replicate the full range of rider postures encountered in real traffic. Future work will incorporate different rider postures to assess their influence on aerodynamic interactions. The bridge model is based on geometric features outlined in the "Design of Main Bridge of Second Penang Bridge in Malaysia" [19]. It includes a simplified road deck, shoulder, and vertical barriers on both sides. A central divider is also included in the model, consistent with the actual bridge structure. While simplified, this divider introduces a local blockage effect and can influence the airflow distribution, especially under crosswind conditions. The potential impact of the divider on the near-vehicle flow field and wake interaction is acknowledged, as it may alter the pressure distribution and lateral aerodynamic forces acting on the motorcycle during overtaking. A Cartesian coordinate system is employed, where the x-axis represents the direction of travel, the y-axis denotes the lateral direction, and the z-axis corresponds to the vertical direction. The effective crosswind velocity (U_{eff}) is determined by combining the motorcycle's forward velocity (U_x) with the crosswind velocity (U_z), forming a yaw angle (β) relative to the motorcycle's motion.

The motorcycle and SUV models are designed to represent typical vehicle geometries, enabling a focus on aerodynamic interactions during overtaking under crosswind conditions. The bridge model represents a simplified structure, consistent with the study's objectives to evaluate aerodynamic effects on vehicles. Figs. 1, 2, and 3 illustrate the geometries of the motorcycle, car, and bridge, respectively. These simplified configurations provide an effective platform for analyzing aerodynamic loads and their implications for vehicle stability and safety. However, it is important to note that simplification introduces limitations in representing fine-scale turbulence interactions and exact body surface pressure distributions that would occur on full-scale, real-world vehicles. As such, while this approach captures dominant aerodynamic behavior, it may underrepresent localized flow phenomena or vibrational effects observed in actual riding conditions.

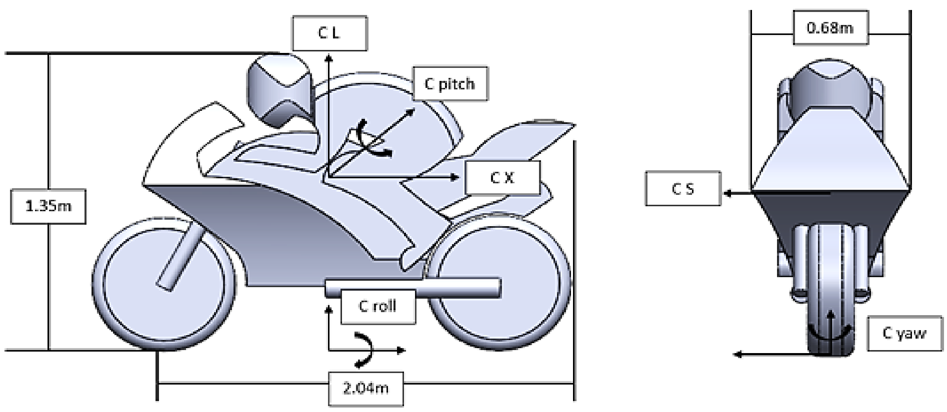

Fig. 1 *Orthogonal view of the motorbike showing the aerodynamic forces and moments, velocity directions, and yaw angle*

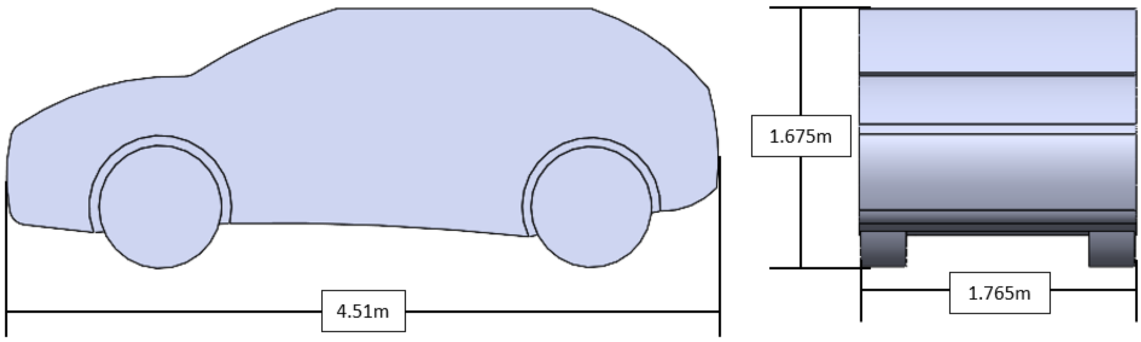

Fig. 2 *Dimensions of simplified car*

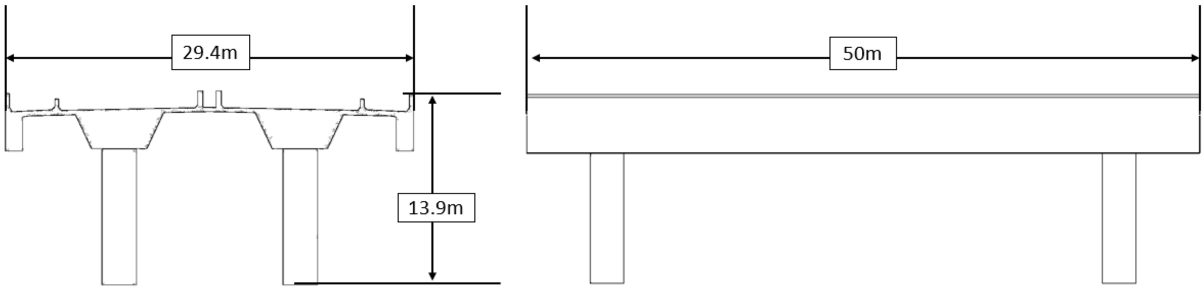

Fig. 3 *Dimensions of simplified bridge*

2.2 Enclosure and Boundary Conditions

Following the development of the project model, the enclosure tool in ANSYS Mechanical was employed to define the surrounding fluid region. This process is essential for enabling the accurate calculation of aerodynamic forces, such as drag force and the drag coefficient [24]. To meet the air domain's boundary conditions, it is imperative to position the model correctly within the enclosure. The dimensions of the enclosure were meticulously selected to ensure the region of interest was adequately represented. This careful selection is crucial for capturing the complete flow field around the model. Key aerodynamic features, including wake regions, vortices, and turbulence, were considered to provide a comprehensive and reliable analysis. In ANSYS simulations, naming boundaries during mesh generation is crucial for identifying surfaces and focusing on key regions of interest [25]. This study defines "velocity inlet" and "crosswind inlet" for fluid entry, a "pressure outlet" for exit, and the vehicle surface for drag calculations. The simulation's boundary conditions were designed to produce accurate and meaningful findings for driving scenarios. At the upstream boundary, a uniform velocity input condition was applied, with inlet velocities.

Furthermore, at the downstream border, a pressure outlet condition enabled the flow to escape freely and was adjusted to atmospheric pressure to imitate an open environment [26]. The surface of the vehicle was represented as a non-slip wall, guaranteeing zero relative fluid velocity to precisely represent drag forces and boundary layer growth. Since there is little interaction between the vehicle and the road surface, the ground plane was also considered a no-slip wall with a constant ground condition [27]. Also, the top of the domain was considered a symmetric boundary condition [28]. Accurate boundary labeling ensures precise representation of fluid interactions and reliable flow behavior analysis. The layout of the enclosure and boundary labels is illustrated in Fig. 4.

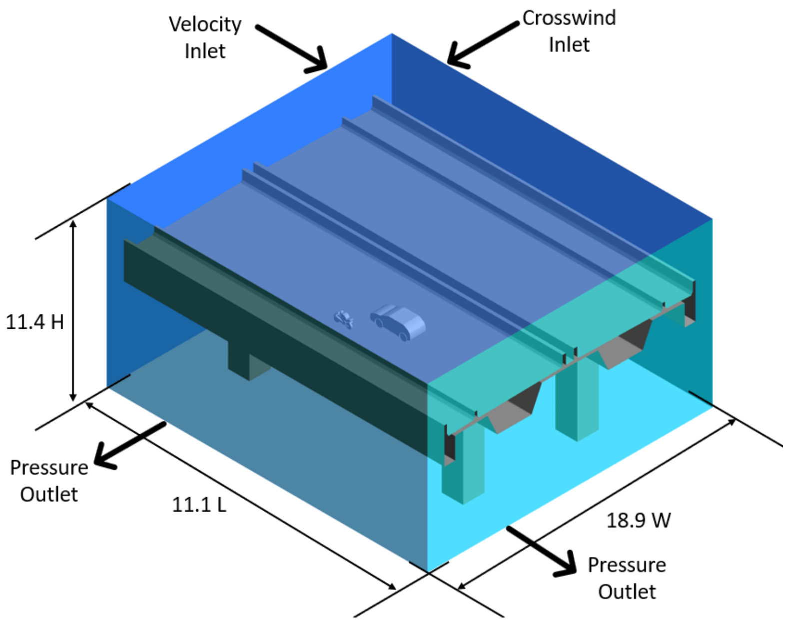

Fig. 4 *Dimension of enclosure for case and name of boundary*

2.3 Mesh Technique

The mesh generation employed a polyhedral meshing technique, which offers enhanced accuracy for complex geometries while minimizing computational resources. The mesh configuration included an element size of 0.015 m, resulting in 8,532,087 cells and 23,139,981 nodes. A smooth transition was implemented in the boundary layer settings with three layers to maintain mesh quality on fluid walls. To capture the intricate geometry of the car and motorcycle on the bridge effectively, local sizing adjustments were applied around critical regions. These settings ensured that the mesh closely represented the physical model, enhancing the potential for accurate aerodynamic calculations. The resulting mesh balanced computational efficiency and geometric fidelity, as shown in Fig. 5.

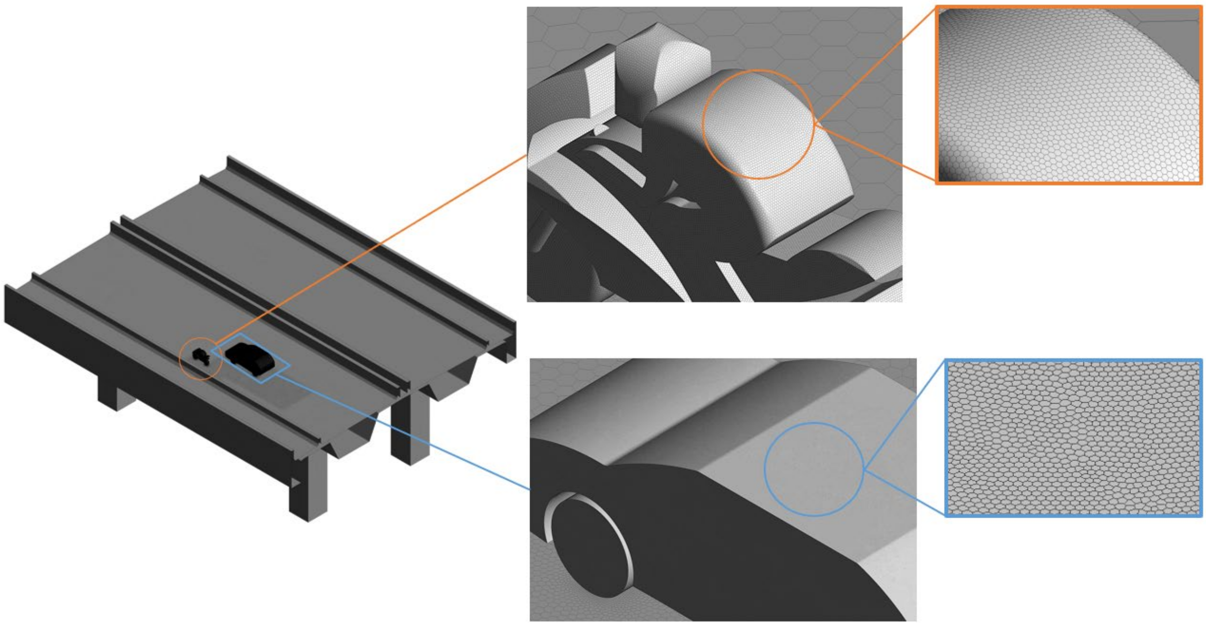

Fig. 5 *Mesh operation of the model*

2.4 Simulation Setup

The mesh setup was followed by configuring the model to calculate the drag coefficient. The Reynolds-Averaged Navier-Stokes (RANS) method was employed to capture flow behavior, with turbulence effects modeled using the K-omega (k-Ω) approach and standard wall functions for accurate near-wall representation [29],[30]. A steady-state RANS model was chosen over more computationally expensive approaches like Large Eddy Simulation (LES) or unsteady RANS (URANS) due to the objective of evaluating time-averaged aerodynamic loads under constant crosswind conditions. Although overtaking and crosswind interactions exhibit inherently transient behavior, the steady-state RANS approach offers a practical balance between computational efficiency and the ability to capture the dominant flow features relevant to drag prediction. This method is especially suitable for preliminary design studies where detailed vortex shedding and transient wake dynamics are of secondary importance. The SIMPLE algorithm ensured stable pressure-velocity coupling [31], while the Green-Gauss cell-based method was used to compute spatial gradients, enhancing the precision of flow field variables. The k-omega (k-Ω) model, known for its accuracy in turbulent flow simulations, was selected over the k-epsilon (k-ε) model for this study. Comprehensive details regarding the solver configuration are presented in Table 1. Simulations were conducted with a constant effective crosswind velocity of 15.2 m/s and a vehicle velocity of 27.78 m/s, resulting in an initial velocity of 43.06 m/s. The simulation environment was modeled as a fluid domain, with the vehicle treated as a void to represent aerodynamic interactions accurately. The crosswind's yaw angle determined the lateral flow velocity (U_z) and frontal flow (U_x), which are stated as:

$$U_x = \cos(\beta)U_{eff} \qquad (1)$$
$$U_z = \sin(\beta)U_{eff}$$

where β is the yaw angle. Table 2 shows the reference value of the setup operation.

Table 1 *Parameters for RANS approach use in simulation*

Parameters	RANS
Model	k-omega
Type	Standard
Wall treatment	Standard wall functions
Solver type	Steady
Number of iterations	500
Pressure velocity coupling	SIMPLE
Spatial discretization (gradient)	Green-Gauss cell based
Pressure	Second order
Momentum	Second order upwind
Turbulent kinetic energy	First order upwind
Specific dissipation rate	First order upwind

Table 2 *Reference value in setup operation*

Detail	Value
Lateral flow velocity, U_z (m/s)	14.73, 21.53, 27.68, 32.99
Frontal flow, U_x (m/s)	40.46, 37.29, 32.99, 27.68
Area (m^2)	0.03418758
Density (kg/m^2)	1.225
Pressure (Pa)	0
Temperature (K)	288.16

2.5 Mesh Refinement Study

In computational fluid dynamics (CFD), the computational domain is discretized into a finite number of grids, where optimal grid design is crucial for achieving accurate results with minimal computational resources. This process involves evaluating various grid configurations to ensure precision and efficiency. For this study, only a simplified motorcycle model was employed to perform a mesh refinement analysis. The governing equations are the Reynolds-Averaged Navier–Stokes (RANS) equations, which describe the conservation of mass and momentum for incompressible turbulent flow. To close the RANS equations, the realizable k–Ω turbulence model was selected due to its robustness in predicting separated flows and wake regions typical in bluff body aerodynamics. The aerodynamic forces were extracted from the simulation to calculate key dimensionless coefficients: the drag coefficient (C_d), which represents the resistance in the direction of motion; the lift coefficient (C_l), which quantifies vertical aerodynamic force; and the side force coefficient (C_s), which indicates lateral aerodynamic loading due to crosswind effects. Additionally, the pitching moment coefficient (C_{pm}) was analyzed to assess rotational stability. The flow was modeled as steady-state, focusing on the time-averaged aerodynamic behavior of the vehicle under crosswind conditions. This approach provides a computationally efficient means of capturing the dominant aerodynamic forces, while simplifying the analysis by neglecting transient effects such as vortex shedding and wake oscillations. Multiple mesh resolutions, varying in type and size, were tested to examine their impact on the total node count, the drag coefficient (C_d), and the pitching moment coefficient (C_{pm}). The results, presented in Table 3, compare C_d and C_{pm} values obtained from ANSYS simulations for different mesh configurations.

Table 3 *Parameters that being used in the simulation*

Parameters	Mesh type		
	Mesh 1	Mesh 2	Mesh 3
Size of curvature & proximity (mm)	20	15	10
Local refinement mesh size (m)	0.01	0.008	0.004
Cell length (mm)	1-16	1-8	1-4
Number of element (cell)	354111	890402	5347332
Number of nodes	978052	1752462	7071303
Drag coefficient, *Cd*	0.556	0.547	0.542
Pitching moment coefficient, *Cpm*	0.021	0.021	0.021
Number of iterations	600	600	600

To validate the accuracy of the simulations, key mesh parameters were systematically varied, and the resulting C_d values were compared against each mesh, as detailed in Table 4 and its mesh refinement graph as shown in Fig. 6. It was observed that finer mesh resolutions significantly improved the accuracy of drag and lift predictions; however, this came at the cost of increased computational demands. Similarly, employing smaller timesteps enhanced the temporal resolution but required substantial computational resources. As a result, a medium mesh resolution is recommended as an optimal compromise, offering a balance between accuracy and computational efficiency [32],[33]. Among the configurations, Mesh 2 was identified as sufficient for predicting aerodynamic loads, as it provided accurate results with minimal computational expense compared to Mesh 3. Specifically, the drag coefficient (C_d) predicted by Mesh 2 was 0.547, which differed by less than 1% from the value obtained using the finer Mesh 3(0.542). This minimal variation indicates that Mesh 2 achieves near mesh-independent results while reducing the computational time required by approximately 40% compared to Mesh 3. This approach ensures that the simulation setup is optimized for efficiency while maintaining reliability in predicting the model's aerodynamic performance.

The study evaluates the influence of mesh resolution on velocity contours and profiles in computational fluid dynamics (CFD) simulations of a motorcycle wake. Fig. 7 illustrates velocity contours at the midplane and velocity profiles for coarse, medium, and fine mesh resolutions. While all mesh resolutions capture the general wake structure, grid errors are evident in simulations with extremely coarse meshes, particularly in regions with significant velocity gradients. These errors manifest as anomalies or irregular waves in the velocity distribution. The medium and fine meshes provide smoother and more continuous velocity profiles compared to the coarse mesh, which struggles to resolve finer flow details. The findings emphasize the critical role of mesh refinement in accurately capturing complex flow features, such as velocity gradients and smaller eddies in the wake region. Although the coarse mesh is sufficient for identifying large-scale flow patterns, achieving detailed accuracy requires a finer mesh. This highlights the trade-off between solution accuracy and computational cost in CFD studies. The results further reinforce the importance of mesh refinement studies to optimize the balance between accuracy and computational efficiency, suggesting that a medium or fine mesh is preferable for reliable wake analysis without excessive computational demands.

Table 4 *Comparison of drag coefficient, Cd in various mesh*

Mesh type	Drag coefficient, C_d	Percentage error (%)
Mesh 1	0.556	-
Mesh 2	0.547	1.62
Mesh 3	0.542	0.91

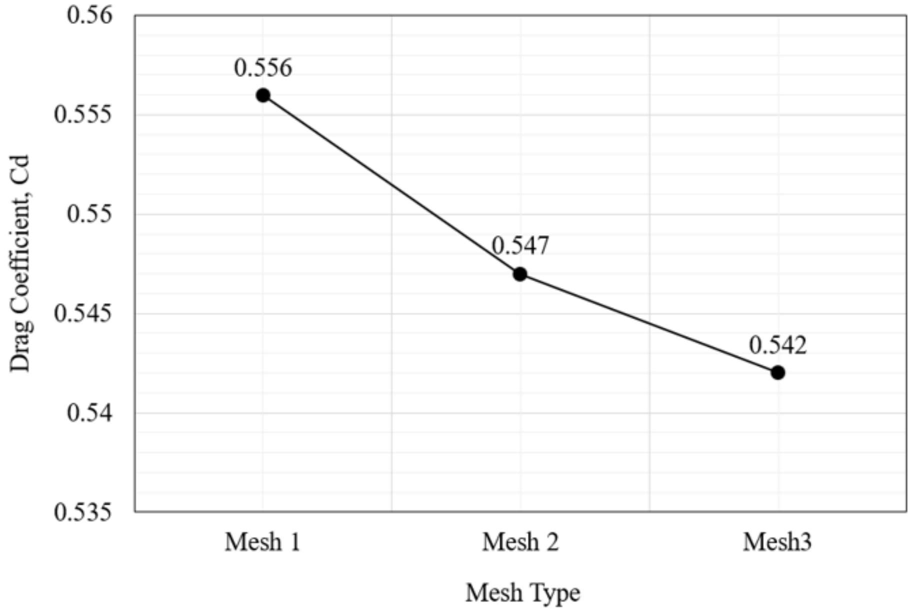

Fig. 6 *Cd graph for different mesh*

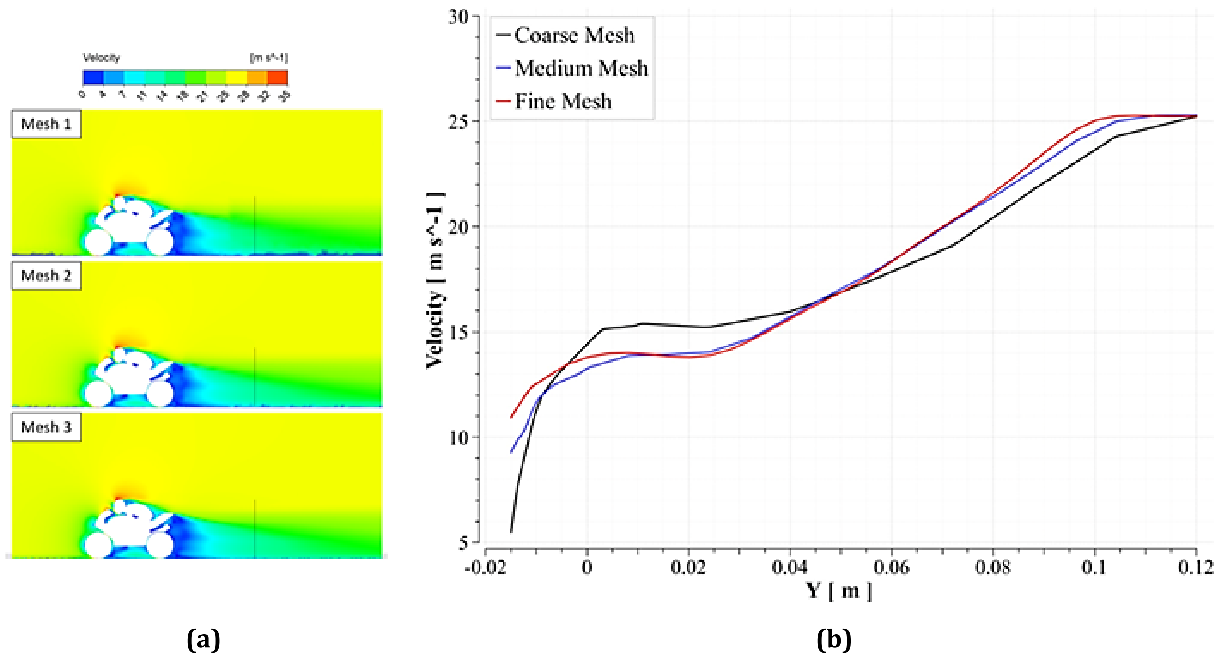

Fig. 7 *(a) Velocity contour with a vertical line behind the motorcycle for different mesh; (b) Velocity graph for different mesh*

2.6 Cases Detail

Two cases need to be taken into account in this project. Each of the cases is reflected based on the objectives stated previously. Case 1 examines how aerodynamic forces affect motorcycles when overtaking in crosswind conditions on the bridge and focuses on the overtaking vehicle's location before, during, and after overtaking. For Case 2, the aerodynamic force between a passing vehicle and the overtaken vehicle will be evaluated at various yaw angles, which are 20°, 30°, 40°, and 50°. The motorcycle's speed will be constant at 100 km/h (27.78 m/s), while the velocity of the crosswind is 55 km/h (15.2 m/s). Fig. 8 shows a car overtaking a motorcycle in different positions before, during, and after overtaking (Case 1). Fig. 9 displays the yaw angles on the vehicles (Case 2).

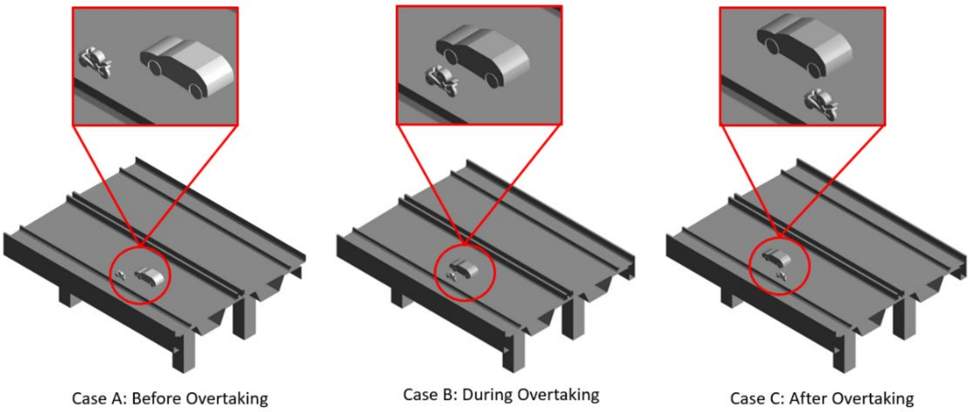

Fig. 8 *Position of motorcycle and car on the bridge in each case*

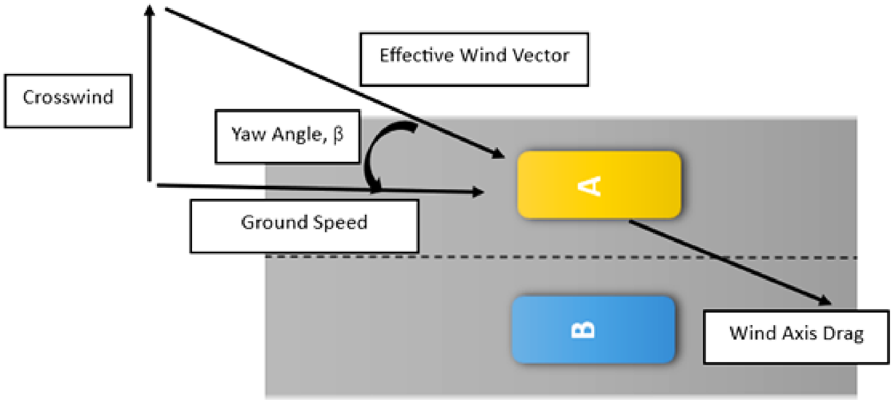

Fig. 9 *Yaw angle of crosswind acting on the vehicles*

3. Results and Discussion

The simulation results focus on crosswind yaw angles (20°, 30°, 40°, and 50°) and three overtaking scenarios involving a Motorcycle (overtaken vehicle) and a Car (overtaking vehicle). The scenarios are divided into three stages: Case A (before overtaking), Case B (during overtaking), and Case C (after overtaking). The findings are evaluated using drag (C_d), lift (C_l), and side force (C_s) coefficients. The results were divided into two primary parts, which are the flow phenomena, including flow structure, pressure distribution, and vortex velocity, and the aerodynamic loads.

3.1 Flow Phenomena

3.1.1 Flow Structure in Crosswind Conditions, β=20°, 30°, 40°, and 50°

The flow structure depicted in Fig. 10 highlights significant aerodynamic interactions between the motorcycle and car during overtaking maneuvers under varying crosswind angles (20°, 30°, 40°, and 50°). Each scenario—(a) before overtaking, (b) during overtaking, and (c) after overtaking—illustrates the impact of crosswind-induced flow behavior on the stability of the motorcycle. At crosswind conditions, β=20°, before overtaking, the flow is relatively uniform, and turbulence is minimal. The motorcycle experiences minor lateral forces due to crosswind, but the aerodynamic disturbance caused by the car ahead is negligible. The flow separation behind the car is small, and its wake does not yet significantly interact with the motorcycle. During overtaking, the motorcycle enters the wake zone of the car. At 20°, the wake is relatively contained, resulting in mild aerodynamic interference. However, the flow's redirection around both vehicles creates a slight increase in side forces on the motorcycle, requiring careful rider adjustments. After overtaking, the motorcycle moves beyond the car's wake. At this crosswind angle, the flow re-stabilizes quickly, and aerodynamic disturbances diminish. The motorcycle regains its original stability, with minimal effort required from the rider. At crosswind conditions, β=30°, the slightly increased crosswind introduces moderate flow separation around the car. The wake extends further downstream, potentially encroaching on the motorcycle's path. The motorcycle encounters an increase in side forces, though stability remains mostly intact.

During overtaking, the flow structure becomes more complex as the wake widens and intensifies. The motorcycle encounters stronger lateral forces, and unsteady flow interactions between the two vehicles create momentary instability. Riders must manage increased rolling moments to maintain control. After overtaking, the wake interaction lingers slightly, causing a brief period of unsteady forces. However, the motorcycle soon exits the wake's influence, allowing stability to return. The impact on control is minimal but noticeable. At crosswind conditions, β=40°, before overtaking, crosswind-induced turbulence intensifies. The car generates a larger wake with more prominent vortices, leading to a noticeable aerodynamic disturbance in the motorcycle's vicinity. The side forces on the motorcycle start to increase, and maintaining stability requires more rider input. Notably, flow separation around the road divider also becomes apparent at this crosswind angle. The separated flow interacts with the wake of the car, contributing additional unsteady aerodynamic effects near the motorcycle. During overtaking, with crosswinds at this angle, the turbulence and wake interaction significantly amplify. The motorcycle experiences sudden shifts in aerodynamic loads due to wake reattachment and detachment. These unsteady forces increase the likelihood of destabilization, demanding heightened rider focus and skill. After overtaking, the wake at this angle persists longer, and the motorcycle continues to experience unsteady aerodynamic forces even after overtaking. The combined effects of the car wake and divider-induced separation delay flow reattachment and prolong instability.

Furthermore, at crosswind conditions, β=50°, before overtaking, high crosswinds at this angle result in a substantial wake zone and highly turbulent flow. The motorcycle is subjected to significant lateral aerodynamic loads even before overtaking begins, increasing the challenge of maintaining a straight trajectory. The road divider plays a more significant role at this yaw angle. Flow separation at the windward edge of the divider generates secondary vortices that interact with the main wake of the overtaking vehicle. This compound wake structure intensifies aerodynamic loading on the motorcycle. The overtaking phase at this angle is critical. The highly turbulent wake envelops the motorcycle, subjecting it to extreme aerodynamic forces, including lift, side forces, and rolling moments. Stability is severely compromised, and even minor rider errors could lead to loss of control. After overtaking, the motorcycle remains in the wake's turbulent zone for an extended period. The divider-induced wake continues to interact with the flow around the motorcycle, delaying recovery of flow uniformity and stability. The rider faces ongoing challenges in counteracting aerodynamic forces, and regaining full stability takes significantly longer. Control efforts must remain vigilant to prevent mishaps.

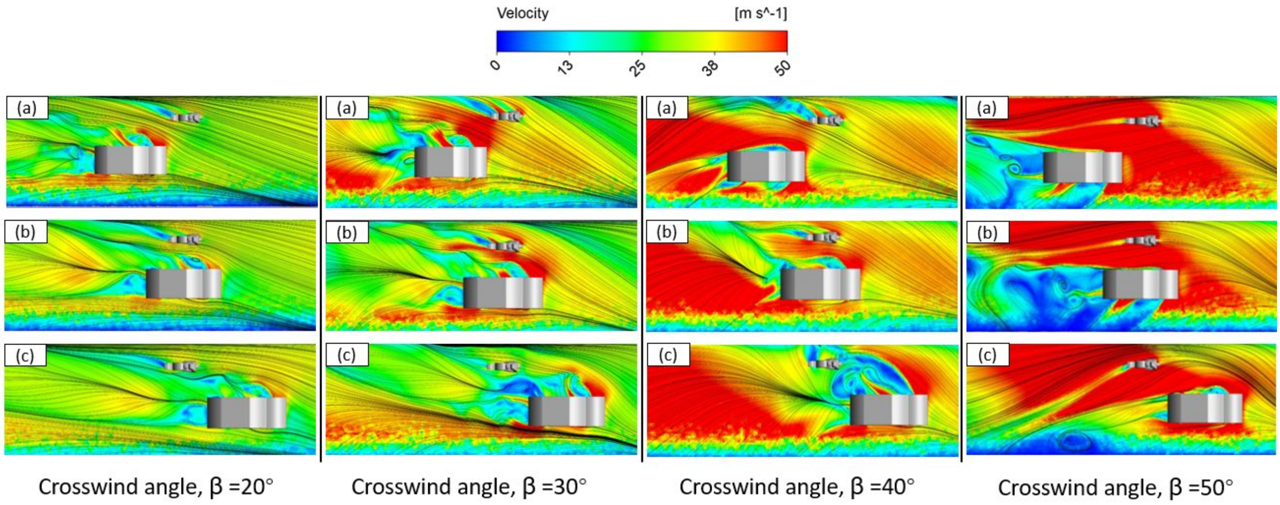

Fig. 10 *Flow structure for motorcycle and car for each case (a) Before overtaking; (b) During overtaking; (c) After overtaking under different crosswind conditions (β=20°, 30°, 40°, and 50°)*

For lower crosswind angles (β = 20° and 30°), the flow remains relatively streamlined, with moderate wake formation and turbulence behind the vehicles. However, during the overtaking phase, the motorcycle is subjected to a slight increase in side forces due to aerodynamic interference, which can momentarily destabilize its lateral motion. While the instability at these angles is manageable, the rider must still compensate for minor deviations caused by the interaction with the wake of the overtaking vehicle. As the crosswind angle increases to 40° and 50°, the flow structure becomes highly turbulent, with amplified wake regions and stronger vortices forming around the vehicles. Additionally, the influence of the road divider becomes more pronounced, contributing to unsteady flow behavior and compound wake interactions. This results in pronounced aerodynamic forces acting on the motorcycle, particularly during and after overtaking. The motorcycle experiences significant rolling moments, lateral forces, and unsteady lift, severely compromising its stability. These forces can lead to sudden deviations in the motorcycle's trajectory, making it challenging for the rider to maintain control. Furthermore, the chaotic flow behavior at higher angles exacerbates the aerodynamic pressure imbalance on the motorcycle, increasing the risk

Int. Journal of Integrated Engineering Vol. 18 No. 3 (2026) p. 31-47

of tipping or skidding. The analysis highlights that the impact on the motorcycle is relatively minor at lower crosswind angles but becomes critical at higher angles, particularly during and after overtaking. These findings emphasize the need for targeted safety measures, such as enhanced bridge design, improved aerodynamic stability in motorcycle design, and rider awareness training, to mitigate the risks of crosswinds during overtaking maneuvers.

3.1.2 Three-Dimensional Vortex Core

The 3D vortex core visualization provides additional insights into the aerodynamic behavior during overtaking maneuvers under varying crosswind angles (20°, 30°, 40°, and 50°) in Fig. 11. At lower crosswind angles (β = 20° and 30°), the vortices generated behind the overtaking vehicle are relatively compact and exhibit limited downstream development. Before overtaking, these vortical structures remain confined near the rear of the car, causing only minimal aerodynamic interference. During overtaking, minor vortex shedding occurs due to the interaction between the wake and the motorcycle, resulting in small-scale, short-lived vortices. These vortices exhibit quasi-steady behavior; their structure and position change gradually, indicating weak unsteady aerodynamic forces acting on the motorcycle. After the overtaking process, the vortices dissipate rapidly, restoring a stable flow field. In contrast, at higher crosswind angles (β = 40° and 50°), the vortex cores are more elongated, intense, and irregular in structure. Before overtaking, strong vortex stretching and lateral diffusion are observed, suggesting increased turbulence and early onset of unsteadiness. As the car approaches the motorcycle, these elongated vortex filaments begin interacting with the motorcycle's frontal and lateral surfaces, generating stronger pressure gradients and fluctuating aerodynamic forces. During overtaking, vortex breakdown and shedding are clear, vortex cores detach from the primary flow path, indicating the presence of highly unsteady, three-dimensional flow structures. These vortex structures do not maintain a fixed shape or location but evolve dynamically as the interaction progresses, contributing to rider instability.

Subsequently, after overtaking, unlike in the lower β cases, the vortex cores remain visible and energetic, confirming that the flow does not immediately return to a steady state. The persistence of these disorganized vortices leads to prolonged aerodynamic disturbances, delaying the recovery of the motorcycle's stable trajectory. These observations suggest that at higher crosswind angles, the vortices generated during overtaking exhibit significantly unsteady behavior, both spatially and temporally. A time-resolved analysis of the flow field (e.g., through transient velocity or vorticity plots) would reveal the oscillatory nature of these vortices, validating that their strength and position fluctuate over time. Such unsteadiness directly affects the aerodynamic loads on the motorcycle, contributing to lateral instability and increased steering correction effort by the rider. Therefore, evaluating the temporal evolution of vortex structures is essential to fully understand the transient aerodynamic behavior during overtaking under strong crosswind conditions. This insight reinforces the need for aerodynamic design optimizations and control strategies that account for unsteady flow effects to improve rider safety.

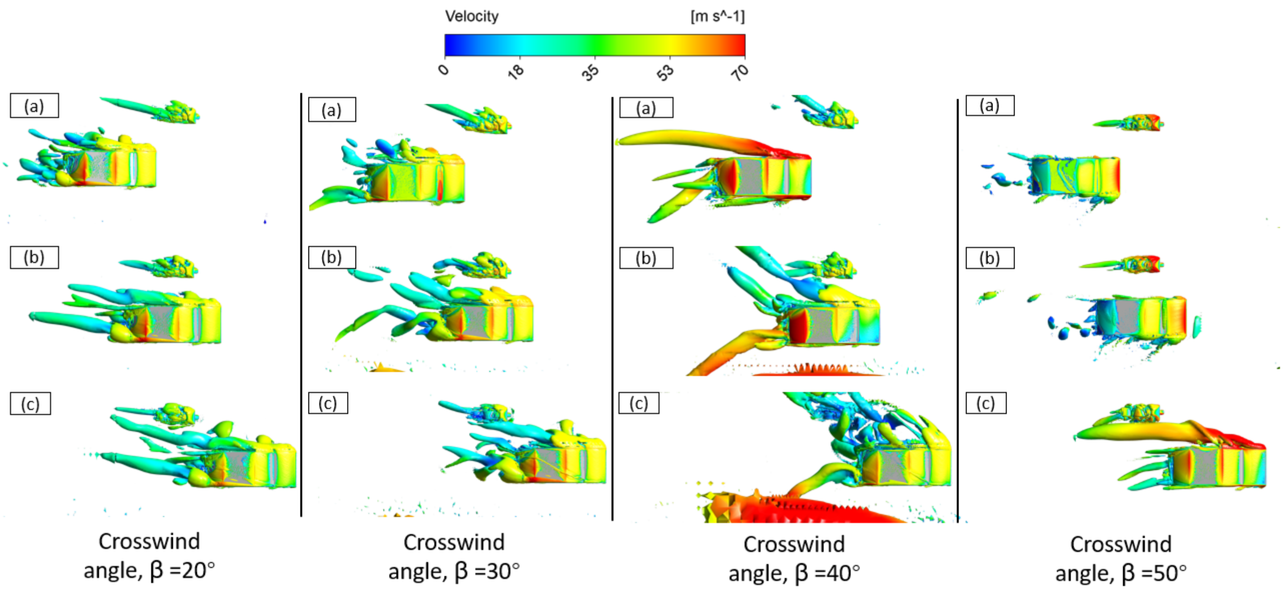

Fig. 11 *Three-dimensional vortex for motorcycle and car for each case (a) Before overtaking; (b) During overtaking; (c) After overtaking under different crosswind conditions (β=20°, 30°, 40°, and 50°)*

3.1.3 Surface Pressure Contour

The surface pressure contour depicted in Fig. 12 highlights significant aerodynamic interactions between the motorcycle and car during overtaking maneuvers under varying crosswind angles (20°, 30°, 40°, and 50°). Across all crosswind angles, distinct pressure distribution patterns are observed on both the car and motorcycle surfaces. Before overtaking, high-pressure zones are evident at the leading edges of both vehicles, particularly on the windward sides, resulting from the combined effects of the oncoming airflow and crosswind interaction. During overtaking, the aerodynamic interference between the car and motorcycle becomes pronounced, causing significant asymmetry in the pressure distribution. This interference creates turbulent regions and increased aerodynamic forces. After overtaking, the pressure distribution begins to stabilize, although high-pressure zones remain near the rear sections of both vehicles, influenced by the trailing wake effects. The influence of crosswind angles on pressure distribution and aerodynamic forces is evident. At β=20°, the pressure gradients are moderate, indicating minimal aerodynamic disturbance. The airflow around both vehicles is relatively smooth, which reduces drag forces and lateral instability. However, as the crosswind angle increases to β=30°, β=40°, and β=50°, the pressure asymmetry intensifies. Notably, at β=40°, cases (a) and (b) exhibit higher surface pressure on the motorcycle compared to β=50°. This suggests that during the before and during overtaking stages, β=40° induces more aerodynamic load on the motorcycle, possibly due to a stronger interaction between the car's wake and the crosswind. However, in case (c), β=50° shows higher surface pressure on the motorcycle, likely due to the intensified turbulence and wake effects as the car moves further ahead, leaving the motorcycle more exposed to the direct crosswind.

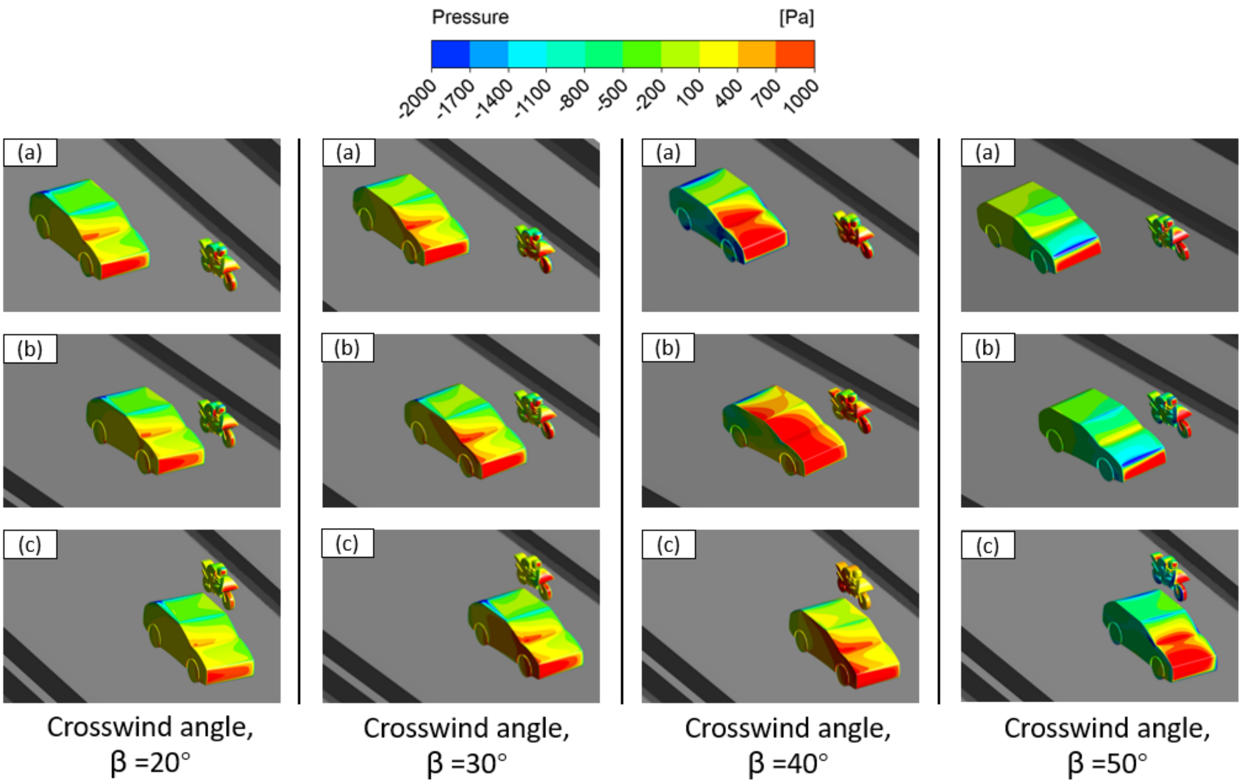

Fig. 12 *Pressure contour for motorcycle and car for each case (a) Before overtaking; (b) During overtaking; (c) After overtaking under different crosswind conditions (β=20°, 30°, 40°, and 50°)*

3.2 Aerodynamic Loads

3.2.1 Drag Force Coefficient

The drag coefficient (C_d) data for the car and motorcycle during overtaking under different crosswind angles (β=20°, 30°, 40°, and 50°) in Fig. 13 reveals distinct aerodynamic trends and impacts. For the car, C_d peaks at β=40° in case (a) (Cd=1.773) due to intensified crosswind interaction but drops sharply at β=50°, while remaining high for cases (b) and (c). This reflects significant changes in flow dynamics during and after overtaking. For the motorcycle, the Cd trends reveal critical aerodynamic challenges. At β=40°, drag is reduced in case (a) (C_d=0.567), suggesting less aerodynamic load before overtaking. However, the motorcycle experiences its highest drag in case (c) at β=50° (C_d=1.406), indicating severe turbulence and wake effects after overtaking. Additionally, during overtaking (case b), C_d steadily increases with higher crosswind angles, highlighting intensified lateral and aerodynamic forces. These trends demonstrate that the motorcycle is more vulnerable to crosswind effects, particularly during and after overtaking. While the increase in drag reflects heightened resistance acting on the motorcycle, it is important to clarify that drag alone, particularly under steady-state conditions, may not directly lead to loss of stability or control. Rather, crosswind-induced side forces and lift are more critical contributors to instability, as they can affect the lateral balance and traction of the motorcycle. Side forces push the motorcycle laterally, potentially displacing it from its lane, while lift reduces the normal force acting on the tires, decreasing grip and making the motorcycle more susceptible to skidding or tipping, especially during rapid maneuvers. Therefore, the observed trends suggest that although drag increases are indicative of turbulent and disturbed flow, it is the combined effects of side force, lift, and unsteady aerodynamic loads—particularly at β = 50° after overtaking—that present the most critical risk to motorcycle control and rider safety.

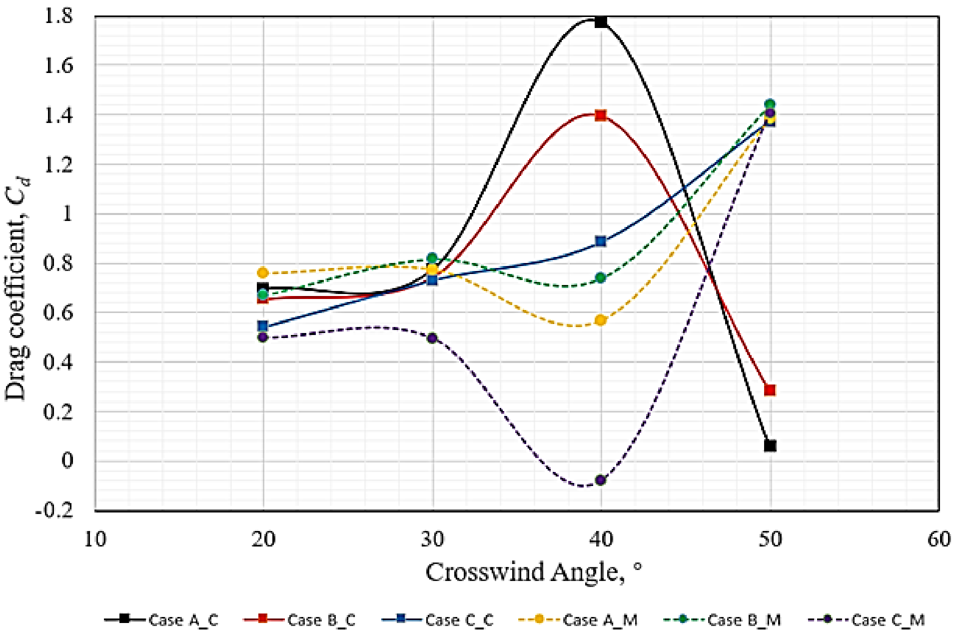

Fig. 13 *Drag coefficient, C_d for motorcycle (M) and car (C) under different crosswind conditions for each case*

3.2.2 Side Force Coefficient

The side coefficient (C_s) trends highlight the impact of crosswind forces on the car and motorcycle in different overtaking scenarios, which is shown in Fig. 14. For the car, C_s values are highest at β=30° in case (b) (C_s=1.418) and case (c) (C_s=1.526), indicating strong lateral forces during and after overtaking. However, C_s decreases significantly at β=40° and β=50°, suggesting reduced lateral aerodynamic effects under extreme crosswind conditions. For the motorcycle, C_s values are most prominent in case (a) at β=30° (C_s=2.296) and case (b) at β=40° (C_s=1.359), reflecting increased crosswind-induced instability before and during overtaking. Interestingly, in case (c) at β=50°, C_s drops to a significant negative value (C_s=−2.634), indicating strong destabilizing forces acting in the opposite direction after overtaking. In real-world riding scenarios, such a sudden change in lateral aerodynamic loading, especially a reversal in force direction, can have serious consequences for rider control. A negative C_s value implies that the lateral force acts opposite to the expected wind direction, potentially causing an unexpected lean or lateral shift of the motorcycle. This can surprise the rider, especially if it occurs during recovery from an overtaking maneuver, leading to oversteering or abrupt corrective input. If not managed correctly, such a force reversal could result in loss of control, lane deviation, or instability during high-speed travel. These findings emphasize the aerodynamic challenges for motorcycles under varying crosswind angles. Elevated C_s values lead to increased lateral forces, reducing stability and maneuverability. In contrast, negative C_s values at higher crosswind angles post-overtaking can cause abrupt changes in stability, posing safety risks that must be addressed through rider training, motorcycle design improvements, or safety protocols for crosswind-prone infrastructure.

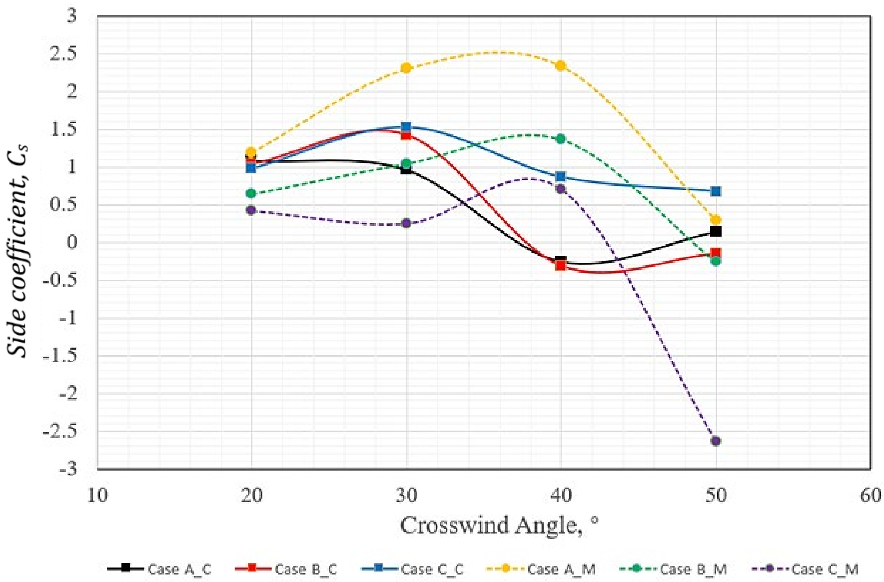

Fig. 14 *Side coefficient, C_s for motorcycle (M) and car (C) under different crosswind conditions for each case*

3.2.3 Lift Force Coefficient

The lift coefficient (C_l) trends highlight the aerodynamic response of the car and motorcycle in different overtaking scenarios, as shown in Fig. 15. For the car, C_l values are highest at β=20° in case (a) (C_l=0.392) and case (c) (C_l=0.519), indicating stronger upward aerodynamic forces before and after overtaking. However, at β=40°, C_l decreases sharply, reaching its lowest point in case (a) (C_l=−1.198) and case (c) (C_l=−0.909), reflecting significant aerodynamic destabilization under extreme crosswind conditions. Interestingly, C_l recovers at β=50° in case (a) (C_l=0.488), suggesting a reduced adverse effect of crosswinds on the car after overtaking. For the motorcycle, C_l values are generally lower compared to the car, reflecting reduced sensitivity to lift-induced aerodynamic forces. In case (a), the highest C_l is observed at β=30° (C_l=0.325), while in case (b), C_l peaks at β=40° (C_l=0.164), indicating moderate aerodynamic forces during overtaking. However, in case (c), C_l decreases to a significant negative value at β=50° (C_l=−0.623), highlighting destabilizing aerodynamic effects acting downward after overtaking. These emphasize the distinct aerodynamic challenges for cars and motorcycles under varying crosswind angles. For cars, elevated C_l values at smaller crosswind angles signify stronger lift forces, potentially reducing stability, particularly during and after overtaking. Conversely, the steep negative C_l values at higher crosswind angles highlight the susceptibility to destabilizing forces, necessitating design enhancements for crosswind resilience. For motorcycles, the relatively lower C_l magnitudes indicate a reduced lift effect, yet the significant negative C_l *post*-overtaking at higher angles reveals potential instability due to wake and crosswind interactions.

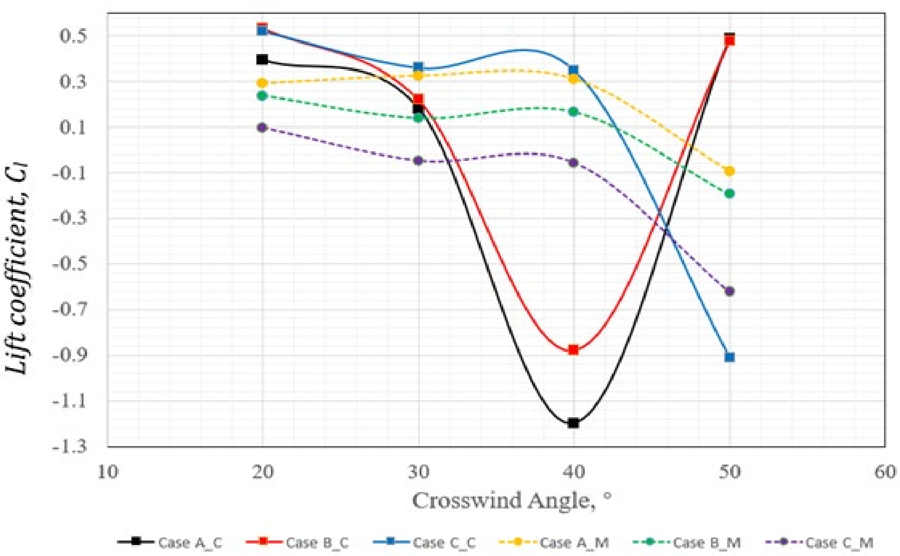

Fig. 15 *Lift coefficient, C_l for motorcycle (M) and car (C) under different crosswind conditions for each case*

4. Conclusions

This study used CFD simulation to examine the aerodynamic interactions between a motorcycle and a car during overtaking maneuvers under varying crosswind conditions, focusing on drag, side, and lift force coefficients at different stages of overtaking. In the initial phase, when the vehicles are far apart, aerodynamic interference is minimal, with forces acting independently and moderate crosswind effects. As the vehicles align side by side, interactions intensify due to wake turbulence from the car, causing asymmetrical pressure distributions, vortex formations, and heightened instability for the motorcycle. Drag and side force coefficients peak at mid-range crosswind angles (30°–40°), increasing by up to 72% and 45%, respectively, destabilizing the motorcycle. Negative drag and side force coefficients at specific angles suggest vortex-induced stabilization, reducing instability by up to 20%. Lift coefficient analysis reveals dynamic changes, with stabilizing negative values at 40° enhancing traction and destabilizing positive values at 50° increasing lift-induced instability. These findings highlight the critical aerodynamic challenges of crosswinds during overtaking, particularly for motorcycles, which are more susceptible due to their smaller size and lighter weight. The results of this study can inform both motorcycle design and rider training programs. For design improvements, manufacturers can optimize fairing shapes and install aerodynamic stabilizers to mitigate the effects of side forces and lift under crosswind conditions. Integrating active aerodynamic systems that adapt to changing yaw angles could also enhance stability.

For rider training, incorporating crosswind response techniques, such as controlled counter steering and body position adjustment, into safety curricula may help riders better anticipate and react to sudden aerodynamic disturbances. Additionally, infrastructure planning, especially for elevated highways and long-span bridges exposed to high wind environments, can benefit from this research. Installing wind barriers, adjusting lane widths, or implementing wind warning systems could reduce exposure during overtaking maneuvers. From a policy perspective, guidelines restricting motorcycle overtaking during high wind warnings could enhance safety. Future research should include experimental validation using wind tunnel tests or full-scale field measurements to corroborate the simulation findings. Furthermore, extending the study to account for rider posture, motorcycle lean angle, and gusting crosswinds could yield more realistic and comprehensive aerodynamic data. Coupling CFD with multi-body dynamics simulations or control systems modeling may also lead to the development of assistive technologies that improve motorcycle handling under adverse aerodynamic conditions.

Acknowledgement

Communication of this research is made possible through monetary assistance by Universiti Tun Hussein Onn Malaysia.

Conflict of Interest

The authors declare that there is no conflict of interest regarding the publication of the paper.

Author Contribution

The authors confirm contribution to the paper as follows: ***study conception and design:*** *Tiong Woei Ting, Izuan Amin Bin Ishak, Mohammad Arafat, Nofrizalidris bin Darlis;* ***data collection:*** *Tiong Woei Ting;* ***analysis and interpretation of results:*** *Tiong Woei Ting, Izuan Amin Bin Ishak, Mohammad Arafat;* ***draft manuscript preparation:*** *Tiong Woei Ting, Izuan Amin Bin Ishak. All authors reviewed the results and approved the final version of the manuscript.*

References

[1] Guo, W. H. & You Lin Xu (2006) Safety analysis of moving road vehicles on a long bridge under crosswind, *Journal of Engineering Mechanics*, *132(4)*, 438-446, https://doi.org/10.1061/(ASCE)0733-9399(2006)132:4(438)

[2] Grm Aleksander & Milan Batista (2017) Vehicle aerodynamic stability analysis under high crosswinds, *Strojniški vestnik-Journal of Mechanical Engineering*, *63(3)*, 191-200, https://www.sv-jme.eu/wp-content/uploads/ns_articles/files/ojs/4095/public/4095-22302-1-PB.pdf

[3] Huang Taiming, Shuya Li, Zhongmin Wan & Zhengqi Gu (2019) Investigation of vehicle stability under crosswind conditions based on coupling methods, *Proceedings of the Institution of Mechanical Engineers, Part D: Journal of Automobile Engineering*, *233(13)*, 3305-3317, https://doi.org/10.1177/0954407018822424

[4] Sima Mikael, Sandor Eichinger, Ander Blanco & Irfan Ali (20150 Computational fluid dynamics simulation of rail vehicles in crosswind: Application in norms and standards, *Proceedings of the Institution of*

Mechanical Engineers, Part F: Journal of Rail and Rapid Transit, *229(6)*, 635-643, https://doi.org/10.1177/0954409714551013

[5] Ma Lin, Xin Chen, Jun Wu & Wanshui Han (2018) Aerodynamic interference mechanism of moving vehicles on a bridge deck in crosswind environment, *Journal of Bridge Engineering*, *23(4)*, 04018011, https://doi.org/10.1061/(ASCE)BE.1943-5592.0001194

[6] Charuvisit S., K. Kimura & Y. Fujino (2004) Experimental and semi-analytical studies on the aerodynamic forces acting on a vehicle passing through the wake of a bridge tower in cross wind, *Journal of Wind Engineering and Industrial Aerodynamics*, *92(9)*, 749-780, https://doi.org/10.1016/j.jweia.2004.04.001

[7] Fintelman Danielle, Hassan Hemida, Mark Sterling & Francois-Xavier Li (2015) A numerical investigation of the flow around a motorbike when subjected to crosswinds, *Engineering Applications of Computational Fluid Mechanics*, *9(1)*, 528-542, https://doi.org/10.1080/19942060.2015.1071524

[8] Arafat Mohammad, Sakthiraaj Rajendran, Izuan Amin Ishak, Muhammad Al & Ain Mat Zin (2024) Effects of crosswinds on the flow structure around a next-generation high-speed train exiting a tunnel, *Jurnal Teknologi (Sciences & Engineering)*, *86(6)*, 29-37, https://doi.org/10.11113/jurnalteknologi.v86.20475

[9] Liu Lining, Yumei Sun, Xuefeng Chi, Guangsheng Du & Meng Wang (2017) Transient aerodynamic characteristics of vans overtaking in crosswinds, *Journal of Wind Engineering and Industrial Aerodynamics*, *170*, 46-55, https://doi.org/10.1016/j.jweia.2017.07.014

[10] Chen Mau-Kuo. (2013) *Use of a rolling road system in crosswind conditions*. Old Dominion University, https://doi.org/10.25777/vng1-yf84

[11] Yudianto Aan, Herminarto Sofyan & Naufal Annas Fauzi (2022) Aerodynamic characteristics of overtaking bus under crosswind: CFD investigation, *CFD Letters* 14(8), 20-32, https://doi.org/10.37934/cfdl.14.8.2032

[12] Hammad Ahmad, Tao Xing, Ahmed Abdel-Rahim, Vibhav Durgesh & John C. Crepeau (2019) Effect of crosswinds on the aerodynamics of two passenger cars crossing each other, *International Journal of Automotive Technology*, *20(5)*, 997-1008, https://doi.org/10.1007/s12239-019-0094-8

[13] Noger C. & E. Van Grevenynghe 2011) On the transient aerodynamic forces induced on heavy and light vehicles in overtaking processes, *International Journal of Aerodynamics*,1(3-4), 373-383, https://doi.org/10.1504/IJAD.2011.038851

[14] Corin R. J., L. He & R. G. Dominy (2008) A CFD investigation into the transient aerodynamic forces on overtaking road vehicle models, *Journal of Wind Engineering and Industrial Aerodynamics*, *96*(8-9), 1390-1411, https://doi.org/10.1016/j.jweia.2008.03.006

[15] Uddin, Mesbah, Arune Dhiren Chellaram & Austin Clay Robinson (2017) CFD investigations of the aerodynamics of vehicle overtaking maneuvers, In *AIP Conference Proceedings*, *1851(1)*, 020085. AIP Publishing LLC, https://doi.org/10.1063/1.4984714

[16] Alonso Estébanez, Alejandro, Juan José del Coz Díaz, Felipe Pedro Álvarez Rabanal, Pablo Pascual Muñoz & Paulino José García Nieto (2018) Numerical investigation of truck aerodynamics on several classes of infrastructures, *Wind and Structures, 26 (1)*.

[17] Ishak Izuan Amin, Amir Khalid, Nik Nur Amyra Adilla Noor Khairullah, Mohammad Arafat, Nurshafinaz Mohd Maruai, and Fadhilah Mohd Sakri (2004) Numerical analysis on the aerodynamic performance of a high-speed train operating on various embankment heights under the influence of crosswinds, *International Journal of Integrated Engineering*, *16(5)*, 3445, https://doi.org/10.30880/ijie.2024.16.05.004

[18] Carsguide Autotrader Media Solutions Pty Ltd (2022). Nissan X-TRAIL Dimensions 2022. https://www.carsguide.com.au/nissan/x-trail/car-dimensions/2022

[19] Man Hou, Liu Bo, Peng Yun Dong & Chang Chung Man (2018) Design of main bridge of second penang bridge in Malaysia, *International Journal of Transportation Engineering and Technology*, *4(2)*, 35-56, https://doi.org/10.11648/j.ijtet.20180402.13

[20] Kamal Muhammad Nabil Farhan, Izuan Amin Ishak, Nofrizalidris Darlis, Daniel Syafiq Baharol Maji, Safra Liyana Sukiman, Razlin Abd Rashid & Muhamad Asri Azizul (2021) A review of aerodynamics influence on various car model geometry through CFD techniques, Journal *of Advanced Research in Fluid Mechanics and Thermal Sciences*, *88(1)*, 109-125, https://doi.org/10.37934/arfmts.88.1.109125

[21] Bella Gino, Stefano Ubertini & Umberto Desideri (2003). *Experimental and computational analysis of the aerodynamic performances of a maxi-scooter*. No. 2003-01-0998. SAE Technical Paper, https://doi.org/10.4271/2003-01-0998

[22] Angeletti Mario, Lucia Sclafani, Gino Bella & Stefano Ubertini (2003) The role of CFD on the aerodynamic investigation of motorcycles, *SAE transactions*, 1103-1111, https://doi.org/10.4271/2003-01-0997

[23] Ghazali Farid & Mohammad Fahmi Abdul Ghafir (2024) Investigation of Different Windshield Designs for Aerodynamic Drag Force in motorcycle, *Progress in Aerospace and Aviation Technology*, *4(1)*, 49-56, https://doi.org/10.30880/paat.2024.04.01.006

[24] Hosain Md Lokman & Rebei Bel Fdhila (2015) Literature review of accelerated CFD simulation methods towards online application, *Energy Procedia*, 75, 3307-3314, https://doi.org/10.1016/j.egypro.2015.07.714

[25] Harlow Francis H. & J. Eddie Welch (1965) Numerical calculation of time-dependent viscous incompressible flow of fluid with free surface, *Physics of Fluids*, *8(12)*, 2182, https://doi.org/10.1063/1.1761178

[26] Wu Chengjun, Jiang Liu & Jie Pan (2014) Influence of surrounding structures upon the aerodynamic and acoustic performance of the outdoor unit of a split air-conditioner, *Chinese Journal of Mechanical Engineering*, *27(4)*, 836-845, https://doi.org/10.3901/CJME.2014.0515.095

[27] Abe, Masato (2015). *Vehicle handling dynamics: theory and application*. Butterworth-Heinemann, https://doi.org/10.1016/B978-1-85617-749-8.00001-5

[28] Favre Tristan & Gunilla Efraimsson (2011) An assessment of detached-eddy simulations of unsteady crosswind aerodynamics of road vehicles *Flow, Turbulence and Combustion, 87(1)*, 133-163, https://doi.org/10.1007/s10494-011-9333-4

[29] Vasilopoulos Konstantinos, Ioannis E. Sarris & Panagiotis Tsoutsanis (2019) Assessment of air flow distribution and hazardous release dispersion around a single obstacle using Reynolds-averaged Navier-Stokes equations, *Heliyon*, *5(4)*, https://doi.org/10.1016/j.heliyon.2019.e01482

[30] Yong Lai Swee, Izuan Amin Ishak, Mohammad Arafat, Nurnida Elmira Othman, Nur Haziqah Shaharuddin & Nurshafinaz Mohd Maruai (2025) CFD analysis on the effects of various train lengths on aerodynamic loads and flow structure for train travelling through various crosswind conditions, *Journal of Advanced Mechanical Engineering Applications*, *6(1)*, 70-79.

[31] Chamkha Ali J. & Younes Menni (2020) Hydrogen flow over a detached V-shaped rib in a rectangular channel." *Mathematical Modelling of Engineering Problems*, *7(2)*, https://doi.org/10.18280/mmep.070202

[32] Yong Lai Swee, Izuan Amin Ishak, Mohammad Arafat, Nurnida Elmira Othman, Nur Haziqah Shaharuddin & Nurshafinaz Mohd Maruai, CFD Analysis on the effects of various train lengths on aerodynamic loads and flow structure for train travelling through various crosswind conditions, *Journal of Advanced Mechanical Engineering Applications*, *6(1)*, 70-79.

[33] Arafat Mohammad, Izuan Amin Ishak & Nurshafinaz Mohd Maruai (2024) Assessment of computational fluid dynamics simulation approach for the aerodynamic performance of small unmanned aerial vehicle propeller, *Engineering Research Express*, *6(4)*, 045578, https://doi.org/10.1088/2631-8695/ad9e6c